AIAA

AIAA 2001-2828

X-38 Experimental Aeroheating At Mach 10

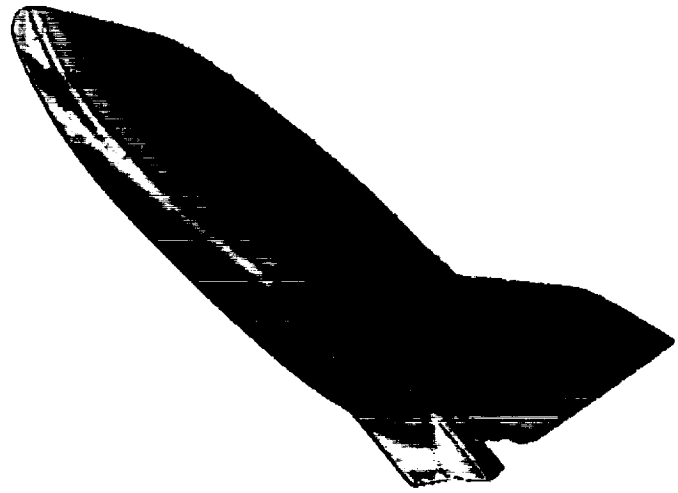

Scott A. Berry,

Thomas J. Horvath,

K. James Weilmuenster,

Stephan J. Alter, and

N. Ronald Merski

NASA Langley Research Center,
Hampton, VA 23681

35th AIAA Thermophysics Conference

11-14 June 2001 / Anaheim, CA

X-38 Experimental Aeroheating at Mach 10

Scott A. Berry,* Thomas J. Horvath,* K. James Weilmuenster,* Stephen J. Alter,* and N. Ronald Merski, Jr.*

ABSTRACT

This report provides an update of the hypersonic aerothermodynamic wind tunnel test program conducted at the NASA Langley Research Center in support of the X-38 program. Global surface heat transfer distributions were measured on 0.0177 and 0.0236 scale models of the proposed X-38 configuration at Mach 10 in air. The parametrics that were investigated primarily include freestream unit Reynolds numbers of 0.6 to 2.2 million per foot and body flap deflections of 15, 20, and 25 deg. for an angle-of-attack of 40-deg. The model-scale variance was tested to obtain laminar, transitional, and turbulent heating levels on the deflected body flaps. In addition, a limited investigation of forced boundary layer transition through the use of discrete roughness elements was performed. Comparisons of the present experimental results to computational predictions and previous experimental data were conducted. Laminar, transitional, and turbulent heating levels were observed on the deflected body flap, which compared favorably to the computational results and to the predicted heating based on the flight aerothermodynamic database.

NOMENCLATURE

h	heat transfer coefficient (lbm/ft^2-sec), $=\dot{q}/(H_{aw} - H_w)$ where $H_{aw} = H_{t2}$
H	enthalpy (BTU/lbm)
k	trip height (in)
L	reference length taken from nose to end of body
M	free stream Mach number
P	pressure (psia)
$\dot{q}$	heat transfer rate (BTU/ft^2-sec)
Re	unit Reynolds number (1/ft)
T	temperature (°R)
t	time (sec)
α	angle of attack (deg)
δ_{BF}	Body flap deflection (deg)

Subscripts

∞	free-stream conditions
t1	reservoir conditions
t2	stagnation conditions behind normal shock
w	wall

INTRODUCTION

The Crew Return Vehicle (CRV), as envisioned by NASA, will provide emergency return-to-earth capability from the International Space Station (ISS) in the event of medical or mechanical problems and Shuttle non-availability (see Brown, 1998). Figure 1 provides an artist's rendering of the CRV docked to the ISS for use in an emergency. The X-38 program led by NASA Johnson Space Center (JSC) seeks to fly a full-scale technology demonstrator to validate key design and operational aspects for the CRV (see Asker, 1996). The X-38 technology demonstrator mission, planned for the early 2003 timeframe, calls for a 28.5 ft long vehicle (designated as V201) to be released by a Shuttle from a high inclination orbit. Following the jettison of a de-orbit engine module, the X-38 will return unpowered (similar to the Space Shuttle) and then use a steerable parafoil, a technology first developed by the Army, for its final descent (discussed by Smith, 1997). Landing will be accomplished on skids rather than wheels. Consistent with the X-38 program's goal to take advantage of available equipment and technology to reduce vehicle development costs by an order of magnitude (see Kandebo, 1998, and Covault, 1998), the shape of the X-38 draws upon a synthesis of work performed by the U.S. government and industry over the last few decades (see Reed, 1997, and Barret, 1999). The initial X-38 shape proposed by NASA JSC was based upon a lifting body concept originally developed and flown during the U.S. Air Force's PRIME (X-23/SV-5D) and PILOT (X-24A) projects in the mid-1960s and early 70's (see Hallion, 1987). The X-24A lifting body shape was initially selected for the CRV mission due to its relatively high hypersonic lift-to-drag ratio (L/D) and volumetric efficiency, and was designated as the X-38 Rev 3.1. The higher L/D translates to larger cross range capability and shorter loiter times in orbit. The current shape (Rev 8.3) departs from the X-23/X-24A and the initial Rev 3.1 in that it reflects changes to the vehicle upper surface to provide for more internal volume and structural stiffness to satisfy launch loads (for possible

* Aerospace Technologist, Aerothermodynamics Branch, Aerodynamics, Aerothermodynamics, and Acoustics Competency, NASA Langley Research Center, Hampton, VA 23681.

launch on top of an expendable rocket). High approach speeds and long rollout distances associated with the low subsonic L/D from this lifting body requires that the landing be augmented with a steerable parafoil (see Dornhiem, 1998). Critical for injured or incapacitated crew, this method permits the CRV to land within close proximity of medical facilities with minimal g-loads.

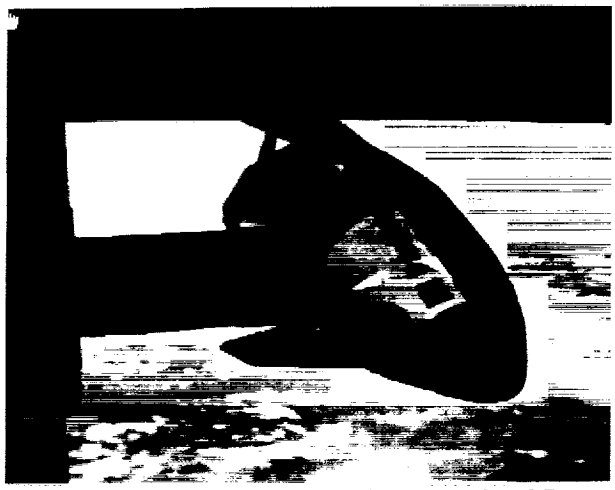

Figure 1. X-38 as a lifeboat for the International Space Station.

Under a NASA/European partnership, Daussault Aviation serves as prime contractor for the development of X-38 flight databases. Labbe, et al. (1999) and Tribot, et al. (1999a and 1999b) are recent examples of this joint effort to derive the X-38 aerothermodynamic database (ATDB). The role of the NASA Langley Research Center (LaRC) Aerothermodynamics Branch (AB) has been to provide hypersonic laminar and turbulent global surface heating and force and moment (F&M) data for CFD validation, and to complement data obtained in European facilities. Results from early LaRC wind tunnel heating tests on Rev 3.1 compared favorably to CFD computations, as detailed by Campbell, et al. (1997b) and Loomis, et al. (1997). Boundary layer transition data was obtained, reported by Berry, et al. (1997), which could be compared to similar Shuttle measurements (see Berry, et al., 1998) in order to support the use of a Re_θ/M_e transition criterion. This criterion is intended for assessment of manufacturing tolerances (step and gaps) of the Thermal Protection System (TPS) tiles, as discussed by Tribot, et al (1999b). Hypersonic aerodynamic screening studies on Rev 3.1 were conducted at LaRC to assess the potential for real gas effects and were reported in Campbell, et al. (1997a). Horvath, et al. (2000) recently provided an overview of LaRC's contributions to the X-38 program. Since the time of these publications, additional aeroheating tests have been completed specifically to characterize the heating levels on the deflected body flaps under laminar, transitional and turbulent conditions.

The thermal environment associated with the X-38 body flaps is considered a challenge from a design perspective due to the complex three-dimensional flowfield and resulting high surface temperatures anticipated in flight. The heating on the X-38 body flap will likely be influenced by three-dimensional flow separations and reattachments, shear layer transition, multiple shock processing of the flow (bow, separation, reattachment), flow expansion and acceleration over the flap edges and through the split gap, etc. As the X-38 flaps are designed as a hot structure (see Muhlrazer, et al., 1999 and Trabandt, et al., 1999), the windward surface temperatures will produce a significant radiative heating exchange between the backside of the flap and aft cavity surfaces. The presence of critical component hardware in this region (flap actuator rod, flap seal) requires an accurate prediction of the environment to insure proper performance and adequate thermal protection.

Early estimates of flap thermal loads at nominal conditions were based upon fully catalytic, turbulent flow (see Campbell, et al., 1996). The actual flap design thermal environment that evolved from these early estimates accounted for additional factors such as vehicle weight growth and higher heating levels associated with a transitional reattaching boundary layer (the "transitional overshoot"). Based upon nominal conditions it was felt that adequate margins existed. These thermal margins were significantly reduced when the operational environment was updated to include trajectory dispersions.

The X-38 program has undertaken a comprehensive computational and experimental effort to more accurately predict the heating environment associated with the windward surface of the deflected body flaps and to insure thermal margins are not exceeded. Under the present NASA/European partnership, previous Mach 6 windward flap heating measurements provided by LaRC were utilized to compliment test results obtained in European facilities. The heating distributions on the flap windward surface were used for developing a thermal design model and flight scaling factors applicable to this localized region, as detailed by Tribot (1999a). The present Mach 10 experimental measurements and corresponding numerical simulations are intended for refinement of this model and to reduce uncertainties.

The purpose of this paper is to present an update of the LaRC experimental program for characterizing the X-38 hypersonic aerothermodynamic environment. Over 50 tunnel runs have been completed in the LaRC 31-Inch Mach 10 Air Tunnel to characterize the state of the

reattaching boundary layer on the deflected body flaps of Rev 8.3 models. The thermographic phosphor technique, which provides global surface heating images, was used to determine heating levels on the body flaps for angles-of-attack and body-flap deflections representative of flight. Parametrics presented here include a range of unit Reynolds numbers (Re) of 0.6 to 2.2 million/ft and body flap deflections (δ_{BF}) of 15, 20, and 25 deg for an angle of attack (α) of 40 deg. These experimental results were complimented with laminar and turbulent computational predictions at wind tunnel conditions of Re=0.6x10^6/ft and 2.2x10^6/ft for α=40-deg and δ_{BF}=20-deg.

EXPERIMENTAL METHOD

Model Description

A sketch of the X-38 Rev 8.3 vehicle is shown in Fig. 2. Three model scales have been built: 0.0177, 0.0236, and 0.0295, which correspond to 6, 8, and 10-in length models, respectively. A rapid prototyping technique was used to build resin stereolithography (SLA) models for each scale with detachable body flaps. The SLA models were then assembled with the desired body flap settings and used as a pattern to create molds from which the ceramic heating models were cast. Symmetric body flaps of 15, 20 and 25-deg were selected based on consideration of the expected deflections in flight. To minimize conduction effects, the body flaps were thickened on the backside to 0.25-in. The flow-through gap between the port and starboard body flaps was maintained. In order to obtain accurate heat transfer data using the one-dimensional heat conduction equation, the cast models were made of a silica ceramic material with low thermal diffusivity and well defined, uniform, isotropic thermal properties. The models were then coated with a mixture of phosphors suspended in a silica-based colloidal binder. The coatings typically do not require refurbishment between runs in the wind tunnel and have been measured to be approximately 0.001 inches thick.

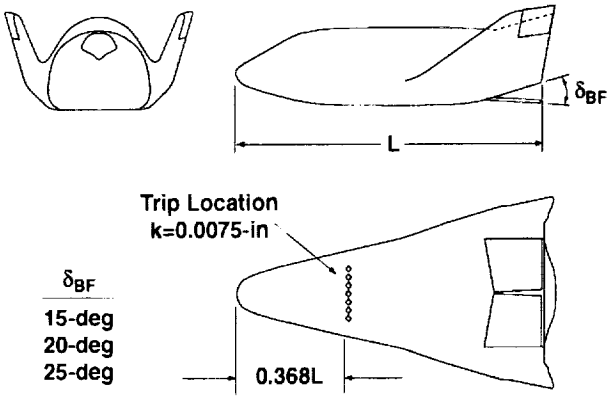

Figure 2. Sketch of X-38 Rev 8.3 model.

Facility Description

The models were tested in the 31-Inch Mach 10 Air Tunnel of the LaRC Aerothermodynamic Facilities Complex. Miller (1992) and Micol (1995) present a detailed description of this blowdown facility, which utilizes dried, heated, and filtered air as the test gas. Typical operating conditions for the Mach 10 tunnel are stagnation pressures ranging from 350 to 1450 psia and stagnation temperatures from 1350 to 1450 °F yielding freestream unit Reynolds from 0.6 to 2.2x10^6/ft. The tunnel has a closed 31- by 31-in. test section with a contoured three-dimensional water-cooled nozzle to provide a Mach number range from 9.6 to 10. A side-loading, hydraulically operated model injection mechanism can place the model into the flow in 0.6 seconds. Figure 3 provides a photograph of the sting-mounted 0.0236-scale X-38 model in the tunnel.

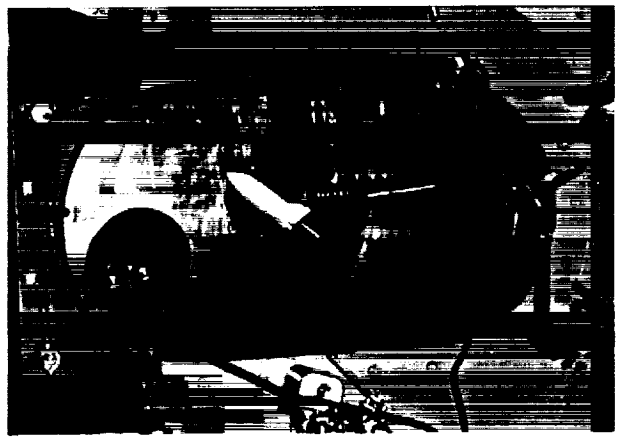

Figure 3. Photograph of the X-38 model installed and injected into the LaRC 31-Inch Mach 10 Tunnel.

Test Conditions

Flow conditions for the 31-Inch Mach 10 Air Tunnel were based on measured reservoir pressures and temperatures and a recent unpublished calibration of the facility. The different model configurations (with varying model scale and body flap deflections) were tested at α=40 deg. A laser alignment system in conjunction with the fiducial marks located along the centerline of the model was used to ensure that sideslip was maintained at zero. Also, a limited number of runs were completed with boundary layer trips, as shown in Fig. 4. These runs were made to ensure fully turbulent boundary layer reattachment on the deflected body flaps utilizing a tripping method similar to that discussed by Berry, et al (1997, 1998). The final trip configuration consisted of a row of 7 diamond-oriented trips, 0.0075-in. high by 0.1-in. square, placed nearly tip-to-tip at the x/L = 0.368 location (see Fig. 2). The nominal flow conditions for the 31-Inch Mach 10 Air Tunnel are listed in Table 1.

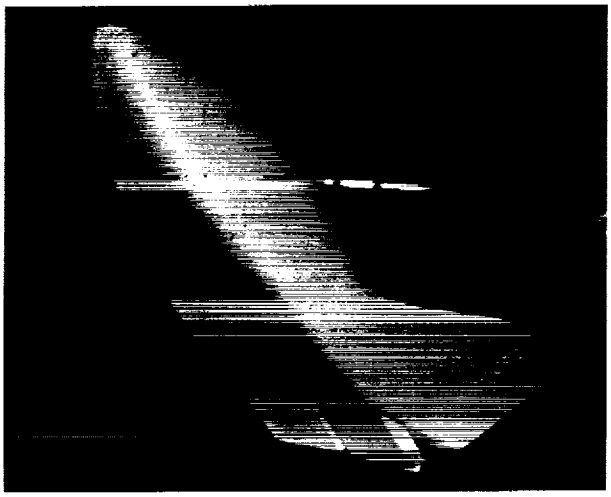

Figure 4. Photograph of the model showing the boundary layer trips on the windward surface.

Test Techniques

The rapid advances in image processing technology occurring in recent years have made digital optical measurement techniques practical in the wind tunnel. One such optical acquisition method is two-color relative-intensity phosphor thermography, which is currently being applied to aerothermodynamic testing in the hypersonic wind tunnels of LaRC. Buck (1989, 1991), and Merski (1998) provide details about the phosphor thermography technique and Berry, et al. (1997, 1998) and Horvath, et al. (2000) provide recent examples of the application of this technique to wind tunnel testing. With this technique, ceramic wind tunnel models are fabricated and coated with phosphors, which fluoresce in two regions of the visible spectrum when illuminated with ultraviolet (UV) light. (Note the UV lights in Fig. 3 used to illuminate the side of the model.) The fluorescence intensity is dependent upon the amount of incident UV light and the local surface temperature of the phosphors. By acquiring fluorescence intensity images with a color video camera of an illuminated phosphor model exposed to flow in a wind tunnel, surface temperature mappings can be calculated on the portions of the model, which are in the camera field of view. (In this case, the camera is located below the tunnel along with several UV lights to illuminate the model windward surface.) A temperature calibration of the system conducted prior to the study provides the look-up tables, which are used to convert the ratio of the green and red intensity images to global temperature mappings. With temperature images acquired at different times during a wind tunnel run, global heat transfer images are computed assuming one-dimensional heat conduction. Phosphor thermography is routinely used in Langley's hypersonic facilities as models that can be fabricated much quicker and more economically than the more conventional techniques provide quantitative global information.

Data Reduction and Uncertainty

Heating rates were calculated from the global surface temperature measurements using one-dimensional, semi-infinite, solid heat-conduction equations, as discussed by Buck (1991) and Merski (1998). Based on Merski (1998), the heat transfer measurements are believed to be accurate to better than ±15 percent. Heating distributions are presented in terms of a normalized heat-transfer. Repeatability for the normalized centerline heat transfer measurements was found to be generally better than ±8 percent.

COMPUTATIONAL METHOD

Prediction Technique

The Langley Aerothermodynamic Upwind Relaxation Algorithm (LAURA) as discussed in detail by Gnoffo, et al. (1989a,1989b,1990) is used for the computations presented in this paper. The LAURA code provided laminar and turbulent solutions of the thin-layer Navier-Stokes equations. The inviscid first-order flux is constructed using the flux-difference splitting scheme of Roe (1981) and entropy fix of Harten (1983) with second-order corrections based on the symmetric total variation diminishing (TVD) scheme of Yee (1985).

Turbulence Model

The turbulence model utilized in LAURA for the present study is based on the two-equation, k-ω model of Wilcox (1993). The equations are fully coupled to the equations for conservation of mass, momentum, and energy. They are implemented to the surface boundary; wall functions are not used. The grid adaptation routine within LAURA is applied to properly resolve the near wall region. The ratio of production to dissipation in the model is limited from above and below by 20 and .05, respectively.

Boundary Conditions

The usual no-slip boundary condition for viscous flow is applied at the wall. The wall temperature is set at a constant value of 540 °R, while freestream conditions are set at points on the outer boundary of the computational domain. The exit plane is set so that the outflow is supersonic.

Grid Generation

The X-38 Rev 8.3 surface grid was constructed from CAD surfaces provided by NASA JSC using GRIDGEN (Steinbrenner, et al., 1989) and VGM (Alter, 1997) and is shown in Fig. 5 along with the body cut locations used for experimental and computational comparisons. The volume grid was constructed using 3DGRAPE/AL

(Sorenson and Alter, 1995). The 20-deg body flap deflection case was selected for computations. The nominal range of body flap deflections during the hypersonic portion of re-entry is 14 to 21-deg and of the two experimental cases within this range, the 20-deg case was more likely to need verification against laminar computations. To simplify the grid geometry, the body flap was modeled as a wedge in order to eliminate the complexity behind the flap. However, due to the flow-through gap between the port and starboard flaps, a large number of grid points were concentrated near the centerline (as shown in Fig. 5) on the forebody in order to adequately define the gap region. Because slideslip is not considered in this report, only half the configuration is used in the computations. Grid sensitivity studies were carried out. The grid as used in these computations is sufficient to resolve the separation region at the flap hinge line and the viscous layer at the wall where the cell Reynolds number is of the order (1). The cell stretching at the edge of the viscous layer is less than 1.2.

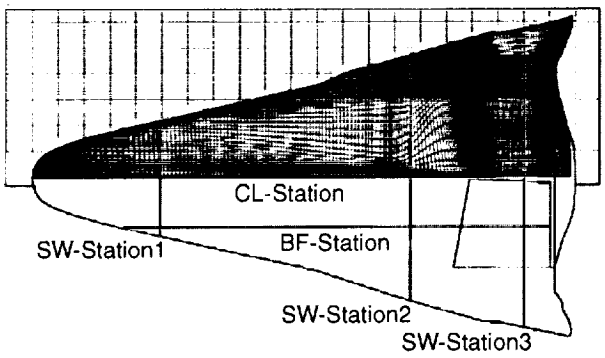

Figure 5. Surface grid and body cut locations.

Computational Conditions

For laminar solutions, the freestream conditions for the 31-Inch Mach 10 Tunnel (see Table 1) for both Re = 0.6 and 2.2 million/ft were used. A turbulent solution was obtained for the Re = 2.2 million/ft freestream conditions starting at x/L=0.07 on the body. Computations of wind-tunnel conditions are based on the assumption of air as a perfect gas.

RESULTS AND DISCUSSION

Global Heating Images

The effect of Reynolds number and boundary layer trips on the windward surface heating images for the 0.0236 scale model for an angle-of-attack of 40-deg is shown in Figs 6, 7, and 8 for body flap deflections of 15, 20, and 25-deg., respectively. For the non-trip cases, the heating levels on the forebody, as well as the size of the separation region in front of the deflected body flaps, remain essentially constant as the Reynolds number is increased for each body flap configuration. This is an indication that the attached forebody flow is laminar. However, for a given body-flap deflection, the heating levels on the deflected body flap generally increase as the Reynolds number is increased. This suggests that the reattaching flow is mostly non-laminar. For instance, for δ_{BF}=20-deg (Fig. 7), the heating level on the body flap is nearly identical for the two lowest Reynolds numbers (suggesting laminar reattachment), but has increased significantly at the highest Reynolds number (suggesting non-laminar reattachment). In order to ensure turbulent heating levels on the deflected body flaps, boundary layer trips were used to force transition on the forebody ahead of the flap separation region. These trip cases, shown in Fig. 6d, 7d, and 8d for k=0.0075-in trips and a Reynolds number of 2.2 million per foot, clearly show the non-laminar flow downstream of the trips, and the resulting reduction in the separation region size due to the energized boundary layer. Also, the body flap reattachment heating appears to move closer to the hinge line. Note that for the largest body flap deflection tested, the trips appear to lower the heating on the body flaps as compared to the untripped case (compare Figs 8c and 8d). This was also observed in the LaRC 20-In Mach 6 Tunnel, as shown in Berry, et al. (1997), where the larger body flap deflections tested provided evidence of a "transitional overshoot." Specifically, the body flap heating was highest when the forebody remained laminar and transition occurred in the shear layer in front of the deflected body flap just prior to reattachment.

Forebody Heating Distributions

The LAURA code was used to provide laminar and turbulent heating predictions for the α=40-deg and δ_{BF}=20-deg case. A comparison of these predictions to the experimental measurements on the X-38 forebody is provided in Fig. 9. The experimental data corresponds to Reynolds numbers of 0.6, 1.1, and 2.2 million/ft and the trip case (k=0.0075-in at x/L=0.368) at Re=2.2x10^6/ft. A ±10% error bar has been place on the experimental data in order to assess the comparisons. The centerline distribution (Fig. 9a) shows the experimental heating levels to be within 10% of the laminar predictions for the cases without a boundary layer trip. For the tripped case, the turbulent computational results downstream of the trip location are slightly higher than the 10% error bar on the experimental data. Similar results are shown in the comparisons at the spanwise locations (SW-Stations 1 and 2 in Fig. 5). Figure 9b provides the heating distribution at SW-Station 1, which is ahead of the boundary layer trips, and shows all four experimental results to be within 10% of the laminar computation.

At SW-Station 2 (Fig 9c), which is just ahead of the separated flow region, the laminar solution is within 10% of the untripped cases, while the tripped case remains below the turbulent prediction. The boundary layer trips appear to be effective, as transition onset is immediate. Furthermore, the plateau of the heating level downstream of the trip would suggest that fully turbulent conditions were reached. However, without further evidence of the validity of either the experimental or computational results, the only conclusion that can be reached about the tripped case is that the flow is non-laminar on the forebody. Note that both the laminar and turbulent computations at SW-Station 2 provide evidence of perturbations near centerline that appear to be related to the high concentration of grid points noted earlier and shown in Fig. 5.

Body Flap Heating Distributions

A comparison of the body flap heating is provided through distributions at BF-Station and SW-Station 3 (as shown in Fig. 5). Figure 10 provides a comparison of the experimental results to predictions at these locations for the δ_{BF}=20-deg case. The measured heating for the Re=0.6x10^6/ft case is shown to agree in both magnitude and distribution to the laminar predictions on the body flap in both the longitudinal cut (Fig. 10a) and the spanwise cut (Fig. 10b). The heating associated with highest Reynolds number case (w/o trips) approaches the level of the turbulent predictions towards the end of the body flap, while the tripped case nearly matches the predictions (within 10%) over the entire body flap, including the location of the reattachment heating. These comparisons suggest that laminar, transitional, and turbulent heating levels have been obtained for the nominal deflected body flap case of 20-deg in the 31-Inch Mach 10 Air Tunnel. Other body flap deflections were also tested, although computational results from LAURA were not available for these cases. Figures 11 and 12 provide the experimental body flap heating levels for the δ_{BF}=15 and 25-deg cases, respectively. For the lowest body flap deflection tested (Fig 11), flow over the body flap appears laminar for all three Reynolds number cases without the trips as the heating distributions roughly collapse, while the tripped case nearly triples the heating level on the body flap. As shown in Fig. 12 for δ_{BF}=25-deg, the heating on the body flap increased with Reynolds number for the untripped cases with the 0.0236 scale model; the tripped result closely matches the highest Re case on the body flap. In order to establish that laminar heating levels were obtained on the body flap, a limited number of runs were conducted with the 0.0177 scale model and these results are also included in Fig. 12. Note that the two Re=0.6x106/ft cases are within the experimental scatter of each other, which may be an indication that the heating levels on the body flap are laminar for these cases. As further evidence that the flow is laminar for these cases, experimental surface streamlines in the vicinity of the body flap for δ_{BF}=25-deg and Re=1.1x10^6/ft are presented in Fig. 13. (The oil-flow technique had been utilized in an earlier entry into the 31-Inch Mach 10 Tunnel for a very limited combination of α, Re, and δ_{BF} with a 0.0177 scale Rev 3.1 model of the X-38.) These surface streamlines can be qualitatively compared to the computed streamlines, shown in Fig. 14 and 15 for the laminar (Re=0.6x10^6/ft) and turbulent (Re=2.2x10^6/ft) cases, respectively. Even though the body flap deflection angles are not the same, the experimental results, in terms of the extent of separation, the location of reattachment, the highly curved flow towards the outboard regions of the flap, more closely resemble the streamlines of the laminar solution.

The X-38 body flap design heating environment for flight is being defined by the program mainly based on experimental results obtained in the 20-Inch Mach 6 Tunnel. Horvath, et al (2000), has presented an overview of these earlier LaRC studies. A comparison of the present measurements at Mach 10 to the Mach 6 results, in terms of heating on the body flap as referenced to a laminar value on the forebody, is provided in Fig. 16. The Mach 6 measurements shown in Fig. 16 include early results that have been provided to the program, and more recently measured results not yet reported. While the turbulent/tripped results between the two tunnels are shown to have excellent agreement, the original results from the Mach 6 tunnel that were thought to be laminar are slightly higher than the Mach 10 results. The earlier Mach 6 tunnel entry utilized the 0.0295 scale model and did not obtained results at the lowest Re available from the tunnel. The more recent Mach 6 results utilized the 0.0177 scale model and many runs at a low enough Re to ensure laminar heating levels agreed well on the body flap. The newer Mach 6 results are shown in Fig. 16 to more closely match the Mach 10 results, which provides stronger evidence of the validity of the laminar, transitional, and turbulent results provided to the X-38 program.

Currently, the nominal body flap deflection angle that is required to trim the vehicle in hypersonic flight is smaller than the deflections that had been tested in the aeroheating studies performed in the LaRC 20-In Mach 6 Air Tunnel and incorporated in the body flap design specification. To provide body flap heating at operational deflections, the X-38 ATDB utilizes a correlation technique that takes advantage of the well-documented interdependence between heating and pressure for flows experiencing shock/boundary-layer

interactions (see, for example Neumann (1972), Holden (1972 and 1978), Hung (1973 and 1977), and Simonides (1993)). As noted in these references, there is a power-law relation between the ratio of the peak values of pressure and heating to their undisturbed values that is a function of the boundary layer state in the vicinity of the interaction. The correlation as currently used is

$$(q/q_{Ref})_{flap}/(q/q_{Ref})_{body} = F\,(p_{flap}/p_{body})^n \qquad (1)$$

where the exponent n (as well as the heating and pressure values) depends on whether the flow is laminar or turbulent and F is a constant that depends on the correlation method. For instance, Holden (1978) has suggested that n=0.7 for laminar heating and n=0.85 for turbulent heating, while F=1. Others have suggested many different combinations of these parameters. The X-38 ATDB is currently using n=1.1 and F=1 for laminar flow, while n=0.8 and F=1.2 for turbulent. Figures 17 and 18 provide a comparison of the laminar and turbulent wind tunnel results to the predicted body flap heating from the ATDB based on the Holden and ATDB methods, respectively. For this paper, the forebody location was selected to be ahead of the separated flow region. The predicted heating results are based on the inviscid flight solutions that provide the pressure ratio term to calculate the right side of equation (1), while the wind tunnel results shown in Fig. 10-12 provide the experimental heating ratio on the left side of equation (1). As the trips did not appear to provide fully turbulent flow on the forebody, the turbulent wind tunnel curves of Fig. 17 and 18 assume the computational value of heating shown in Fig. 10 as the turbulent forebody value. Based on the comparison shown in Fig. 17 and 18, the correlation method currently employed by the X-38 ATDB provides a better representation of the present Mach 10 experimental data than the Holden method.

CONCLUDING REMARKS

An update of the hypersonic aerothermodynamic wind tunnel test program conducted at the NASA Langley Research Center in support of the X-38 program is presented. Global surface heat transfer distributions were measured on several scale models of the current X-38 flight vehicle at Mach 10 in air. The primary parametrics investigated include freestream unit Reynolds numbers from 0.6 to 2.2 million per foot and body flap deflections of 15, 20, and 25 deg for an angle-of-attack of 40 deg. Boundary layer trips were utilized to ensure turbulent heating levels on the deflected body flaps. The Reynolds number range available with the Mach 10 facility along with the boundary layer trips was sufficient to produce laminar, transitional, and turbulent boundary layers on the deflected body flaps. Comparisons of the present experimental results to computational predictions were performed and agreed within the experimental uncertainty. The body flap heating was on the order of two times the reference levels under laminar conditions and as much as four times the reference under turbulent conditions. The methodology employed by the X-38 program to predict the heating levels on the body flap in flight was shown to represent the Mach 10 experimental data.

REFERENCES

Alter SJ. 1997. The Volume Grid Manipulator (VGM): A Grid Reusability Tool. NASA CR-4772

Asker JR. 1996. For Myriad Woes, NASA Calls X-38 to the Rescue. *Av. Wk. & Sp. Tech.* 145(20):70-1

Barret C. 1999. Lifting Body Stability and Control. *NASA TM-1999-209255*

Berry SA, Horvath TJ, Roback VE, Williams GB. 1997. Results of Aerothermodynamic and Boundary-Layer Transition Testing of 0.0362-Scale X-38 (Rev. 3.1) Vehicle in NASA Langley 20-Inch Mach 6 Tunnel. *NASA TM-112857.*

Berry SA, Bouslog SA, Brauckmann GJ, Caram JM. 1998. Shuttle Orbiter Experimental Boundary-Layer Transition Results with Isolated Roughness. *J. of Spacecr. Rockets* 35(3):241-248

Brown D. 1998. Manning the Lifeboats on the International Space Station. *Launchspace* 3(2):20-2

Buck GM. 1989. Automated Thermal Mapping Techniques Using Chromatic Image Analysis. *NASA-TM-101554*

Buck GM. 1991. Surface Temperature/Heat Transfer Measurement Using A Quantitative Phosphor Thermography System. *AIAA Pap.* 91-0064

Campbell CH, Caram JM, Li CP, Madden CM. 1996. Aerothermodynamic Environment Definition for an X-23/X-24A Derived Assured Crew Return Vehicle. AIAA Paper 96-1862

Campbell CH, Caram JM, Berry SA, Horvath TJ, DiFulvio M. 1997a. Overview of X-38 Hypersonic Wind Tunnel Data and Comparison with Numerical Results. *AIAA Pap.* 97-0567

Campbell CH, Caram JM, Berry SA, Horvath TJ, Merski NR, Loomis MP, Venkatapathy E. 1997b. An Overview of X-38 Hypersonic Aerothermodynamic Wind Tunnel Data and Comparison with Numerical Results. *AIAA Pap.* 97-2475

Covault C. 1998. Second X-38 Set for Flight. *Av. Wk. & Sp. Tech.* 149(9):58

Dornhiem MA. 1998. X-38 Transitions from Lifting Body to Parafoil. *Av. Wk. & Sp. Tech.* 148(12):92

Gnoffo PA, Gupta RN, Shinn J. 1989a. Conservation Equations and Physical Models for Hypersonic Air Flows in Thermal and Chemical Nonequilibrium. *NASA TP-2867*

Gnoffo PA. 1989b. Upwind-Biased, Point-Implicit Relaxation Strategies for Viscous Hypersonic Flows. *AIAA Pap.* 89-1972

Gnoffo PA. 1990. An Upwind Point Implicit Relaxation Algorithm for Viscous Compressible Perfect-Gas Flows. *NASA TP-2953*

Hallion RP, ed. 1987. *The Hypersonic Revolution: Eight Case Studies in the History of Hypersonic Technology*. Special Staff Office, Aeronautical Systems Division Wright-Patterson Air Force Base

Harten A. 1983. High Resolution Schemes for Hyperbolic Conservation Laws. *J Comp. Phys.* 49(3):357-93

Holden MS. 1972. Shock Wave Turbulent Boundary Layer Interaction in Hypersonic Flow. AIAA Pap. 72-74

Holden MS. 1978. A Study of Flow Separation in Regions of Shock Wave Boundary Layer Interaction in Hypersonic Flow. AIAA Pap. 78-1169

Horvath TJ, Berry SA, Merski NR, Fitzgerald SM. 2000. X-38 Experimental Aerothermodynamics. *AIAA Pap.* 2000-2685

Hung FT. 1973. Interference Heating Due to Shock Wave Impingements on Laminar Boundary Layers. AIAA Pap. 73-678

Hung FT. 1977. Three-Dimensional Shock Wave Interference Heating Prediction. AIAA Pap. 77-756

Kandebo SW. 1998. Vista F-16 Tests Preview X-38 Flight Controls. *Av. Wk. & Sp. Tech.* 149(16):41

Labbe SG, Perez LF, Fitzgerald SM, Longo JMA, Rapuc M. 1999. X-38 NASA/DLR/ESA-Dassault Aviation Integrated Aerodynamic and Aerothermodynamics Activities. In *Proc. Atmospheric Reentry Vehicle and Systems Int. Symp.*

Loomis MP, Venkatapathy E, Papadopoulos P, Davies CB, Berry SA, Horvath TJ, Campbell CH. 1997. Aeroheating and Aerodynamic CFD Validation and Prediction for the Computational/ Experimental Aeroheating Predictions for the X-38 Program. *AIAA Pap.* 97-2478

Merski NR. 1998. Reduction and Analysis of Phosphor Thermography Data with the IHEAT Software Package. *AIAA Pap. 98-0712*

Micol JR. 1995. Hypersonic Aerodynamic/ Aerothermodynamic Testing Capabilities at Langley Research Center: Aerothermodynamic Facilities Complex. *AIAA Pap.* 95-2107

Miller CG. 1990. Langley Hypersonic Aerodynamic/ Aerothermodynamic Testing Capabilities - Present and Future. *AIAA Pap.* 90-1376

Muhlrazer A, Frohlich A, Wildenrotter K. 1999. Design, Material and Manufacturing Aspects of the X-38 Body Flaps. In Proc. Atmospheric Reentry Vehicle and Systems Int. Symp. in Arachon, France

Neumann RD. 1972. Special Topics in Hypersonic Flow. In "Aerodynamic Problems of Hypersonic Vehicle", AGARD LS 42

Reed RD. 1997. Wingless Flight The Lifting Body Story. NASA SP-4220

Roe PL. 1981. Approximate Riemann Solvers, Parameter Vectors, and Difference Schemes. J Comp. Phys. 43:357-72

Simeonides G. 1993. Hypersonic Shock Wave Boundary Layer Interactions Over Simplified Deflected Control Surface Configurations. In "Special Course on Shock-Wave/Boundary-Layer Interactions in Supersonic and Hypersonic Flows", AGARD Report 792

Smith BA. 1997. Weather May Hamper X-38 Drop Tests. Av. Wk. & Sp. Tech. 147(24):33

Sorenson RL, Alter SJ. 1995. 3DGRAPE/AL: The Ames/Langley Technology Upgrade. NASA CP-3143

Steinbrenner JP, Chawner JR, Fouts CL. 1989. The GRIDGEN 3D Multiple Block Grid Generation System. WRDC-TR-90-3022

Trabandt U, Schmid T, Reinkober H, Ritter H. 1999. Light-Weight CMC TPS for Future RLV Applied On X-38 Nose Skirt. In Proc. Atmospheric Reentry Vehicle and Systems Int. Symp.in Arachon, France

Tribot JP. 1999a. X-38 Aerothermodynamic Data Base. Dassault Aviation Document DGT 77469

Tribot JP, Tran P, Pallegoix JF, Orlowski M, Bruck S, Andres OP, Fitzgerald SM. 1999b. X-38 Aerothermodynamics. In Proc. Atmospheric Reentry Vehicle and Systems Int. Symp. in Arachon, France

Wilcox DC. 1993. Turbulence Modeling for CFD, DCW Industries, La Canada, CA.

Yee HC. 1985. On Symmetric and Upwind TVD Schemes. NASA TM-86842

Table 1. Nominal flow conditions for LaRC 31-Inch Mach 10 Air Tunnel.

Re_∞ (x106/ft)	M_∞	Pt1 (psi)	Tt1 (°R)	Ht1 (BTU/lbm)	Pt2 (psi)
0.6	9.7	350	1770	442	1.2
1.1	9.8	720	1820	457	2.4
2.2	9.9	1450	1820	458	4.5

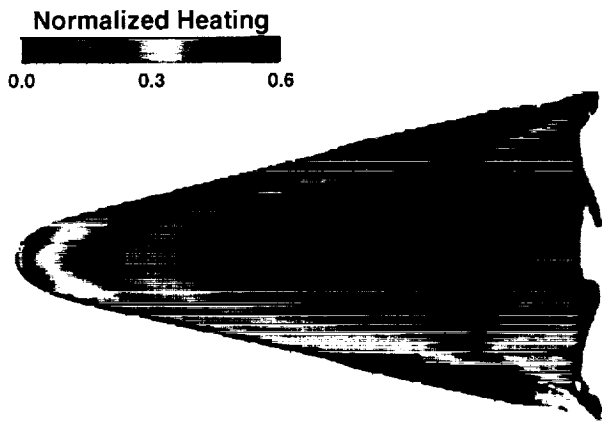

a) Re=0.6x106/ft

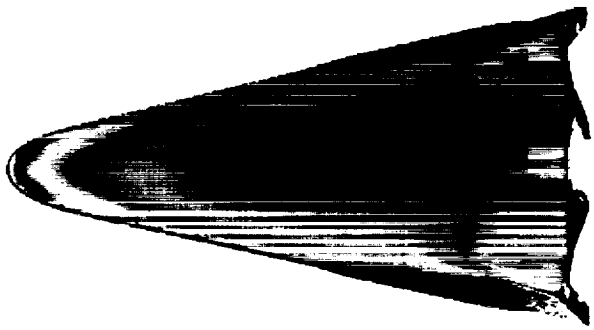

b) Re=1.2x10^6/ft

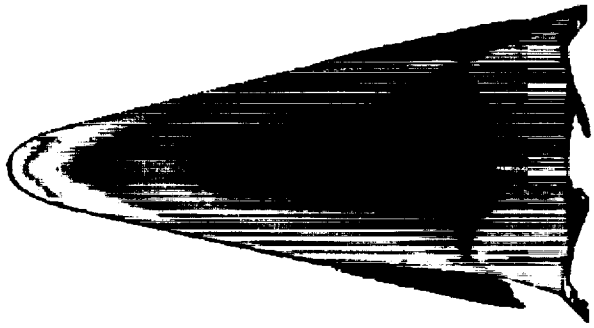

c) Re=2.2x10^6/ft

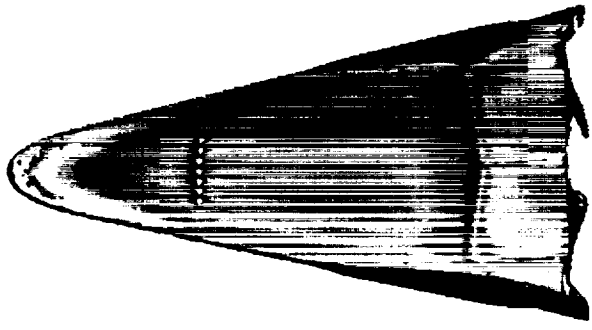

d) Re=2.2x10^6/ft, k=0.0075-in

Figure 6. Effect of unit Reynolds number and trips on global heating for M_∞=10, α=40-deg, and δ_{BF}=15-deg.

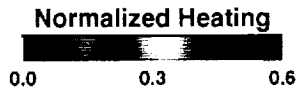

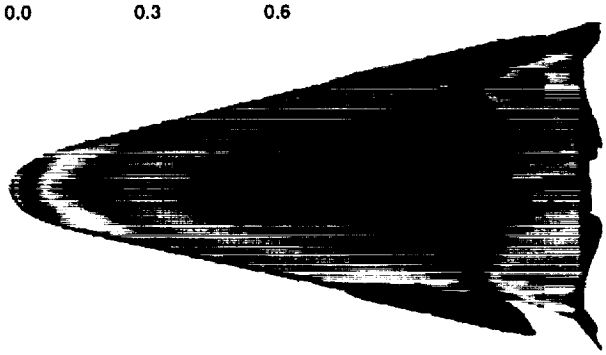

a) Re=0.6x10^6/ft

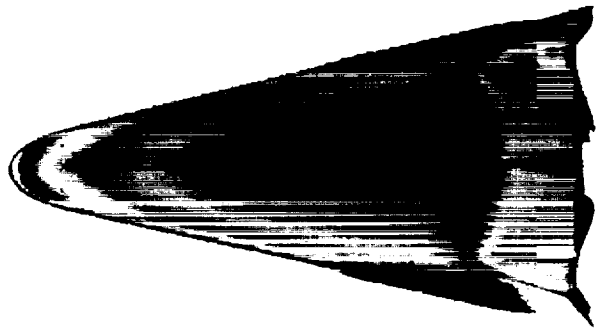

b) Re=1.2x10^6/ft

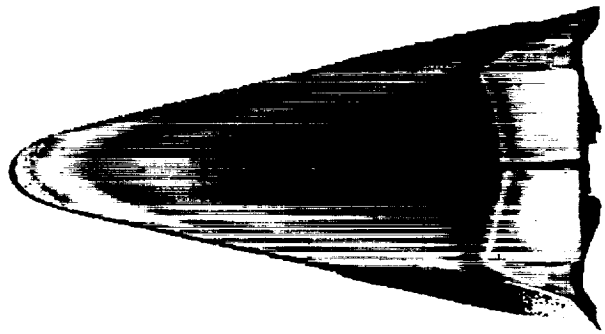

c) Re=2.2x10^6/ft

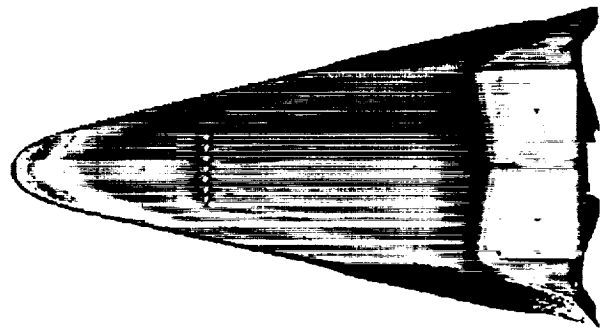

d) Re=2.2x10^6/ft, k=0.0075-in

Figure 7. Effect of unit Reynolds number and trips on global heating for M_∞=10, α=40-deg, and δ_{BF}=20-deg.

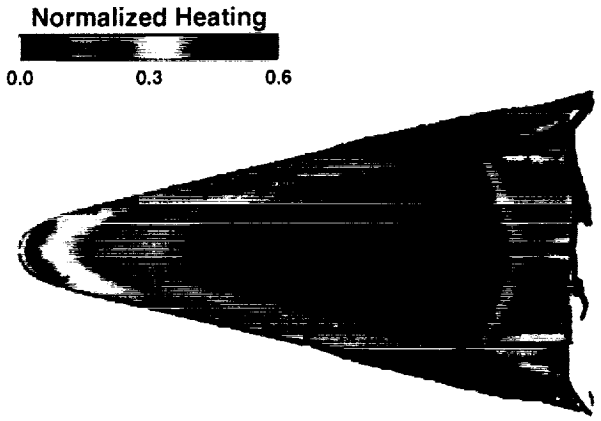

a) Re=0.6x10^6/ft

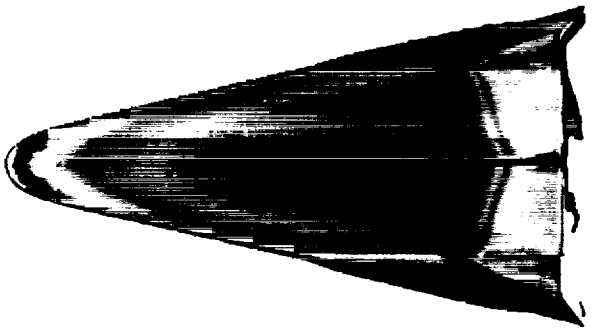

b) Re=1.2x10^6/ft

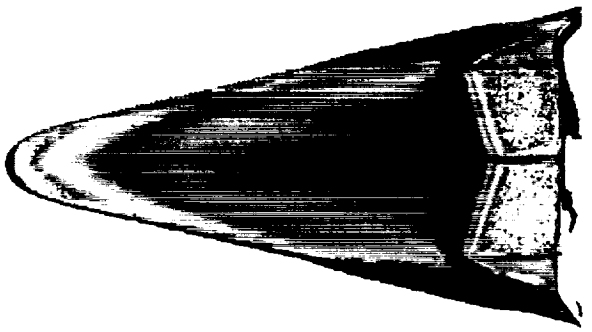

c) Re=2.2x10^6/ft

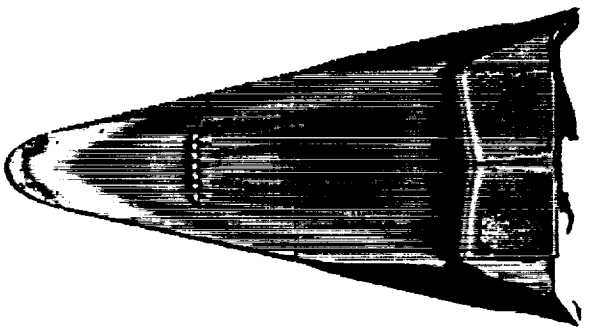

d) Re=2.2x10^6/ft, k=0.0075-in

Figure 8. Effect of unit Reynolds number and trips on global heating for M_∞=10, α=40-deg, and δ_{BF}=25-deg.

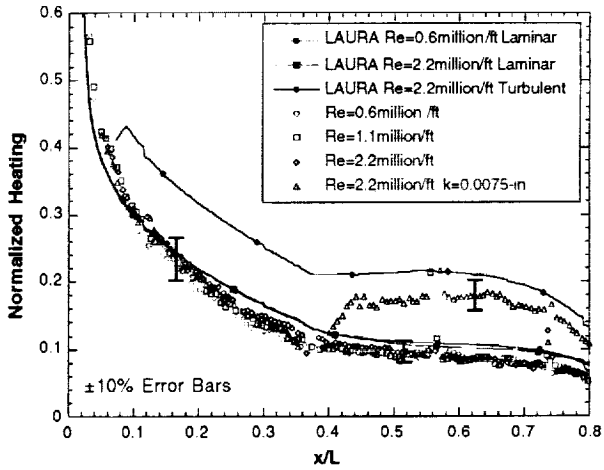

a) Centerline distribution

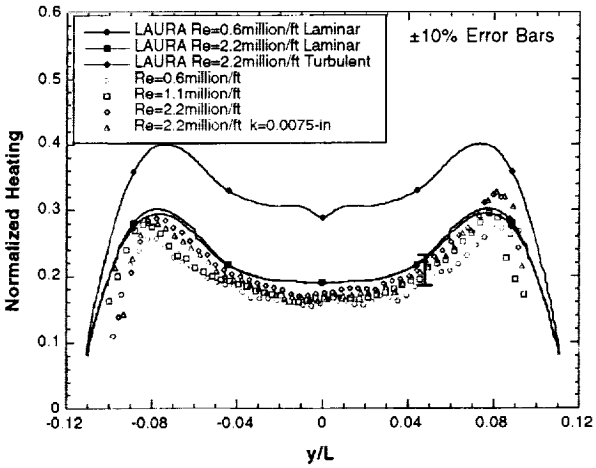

b) Spanwise distribution at SW-Station 1

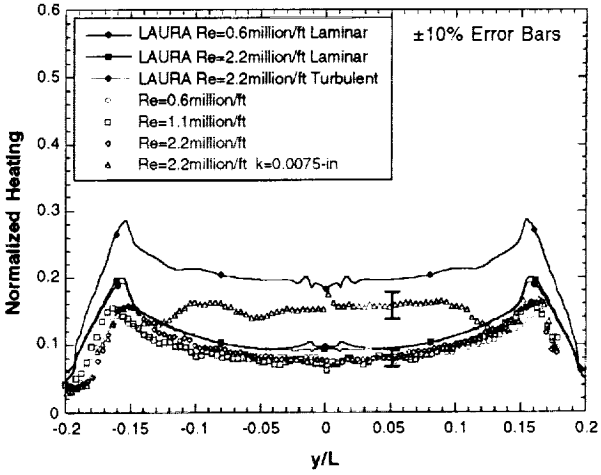

c) Spanwise distribution at SW-Station 2

Figure 9. Comparisons of forebody heating results to predictions for M_∞=10, α=40-deg.

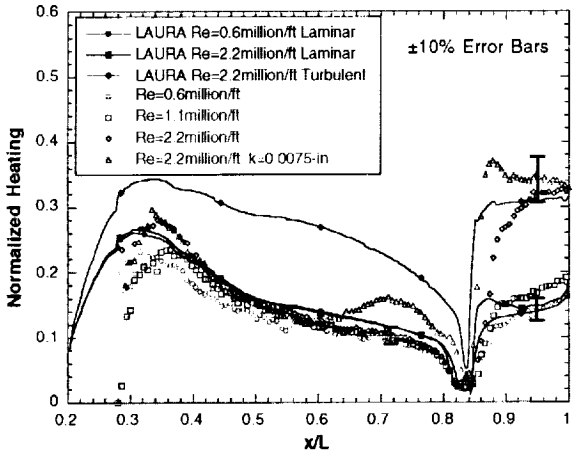

a) Longitudinal distribution at BF-Station

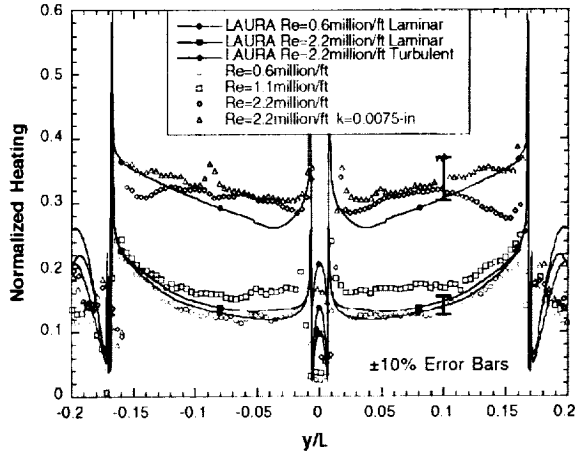

b) Spanwise distribution at SW-Station 3

Figure 10. Comparisons of heating results to predictions for M_∞=10, α=40-deg, and δ_{BF}=20-deg.

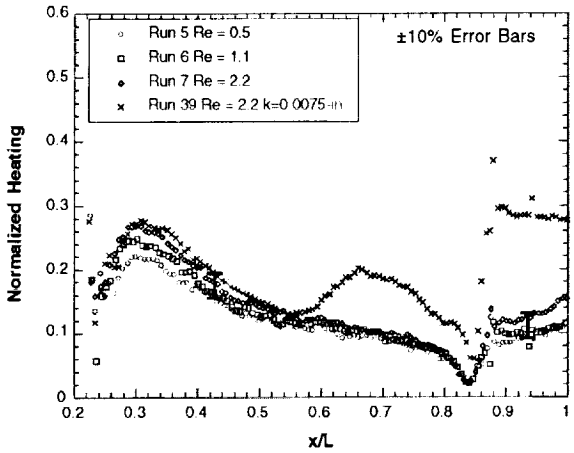

a) Longitudinal distribution at BF-Station

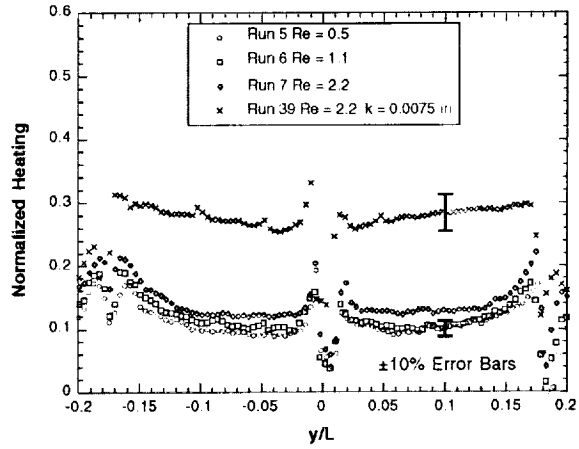

b) Spanwise distribution at SW-Station 3

Figure 11. Comparisons of heating results for M_∞=10, α=40-deg, and δ_{BF}=15-deg.

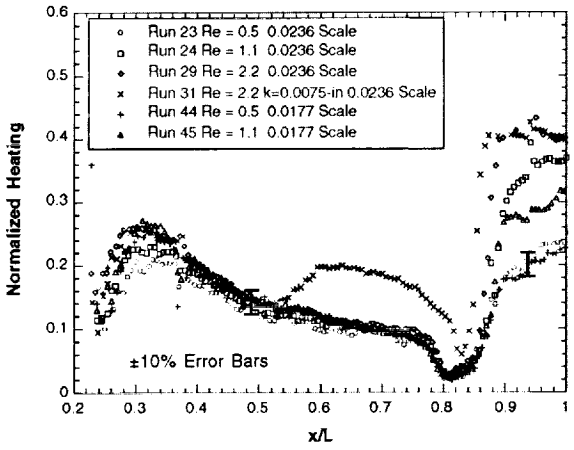

a) Longitudinal distribution at BF-Station

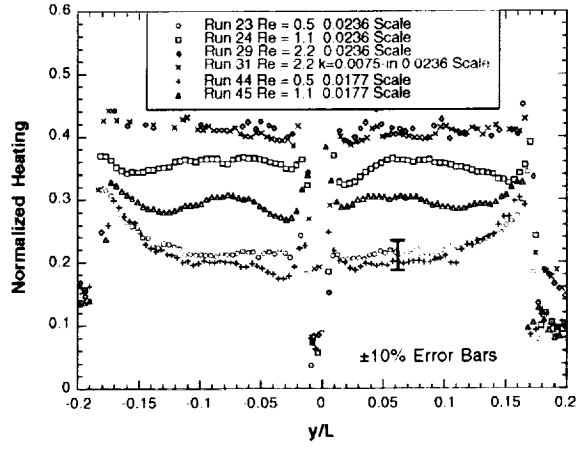

b) Spanwise distribution at SW-Station 3

Figure 12. Comparisons of heating results for M_∞=10, α=40-deg, and δ_{BF}=25-deg.

Figure 13. Experimental surface streamlines for α=40-deg, Re=1.1x10^6/ft and δ_{BF}=25-deg.

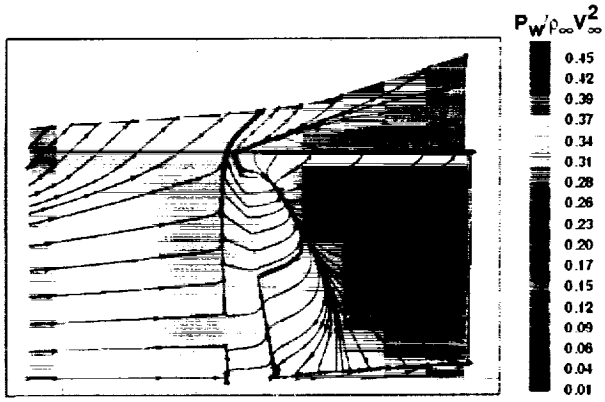

Figure 14. Surface streamlines and pressures from laminar predictions for α=40-deg, Re=0.6x10^6/ft and δ_{BF}=20-deg.

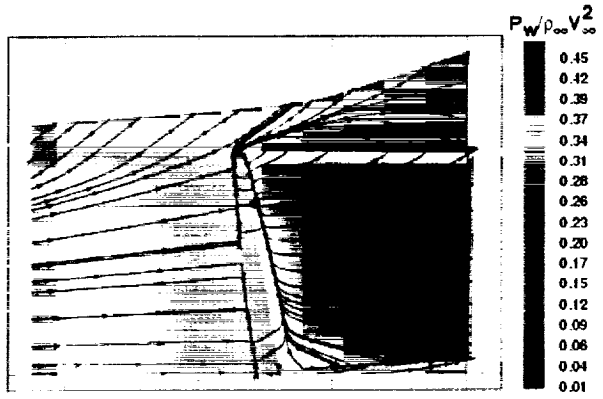

Figure 15. Surface streamlines and pressures from turbulent predictions for α=40-deg, Re=2.3x10^6/ft and δ_{BF}=20-deg.

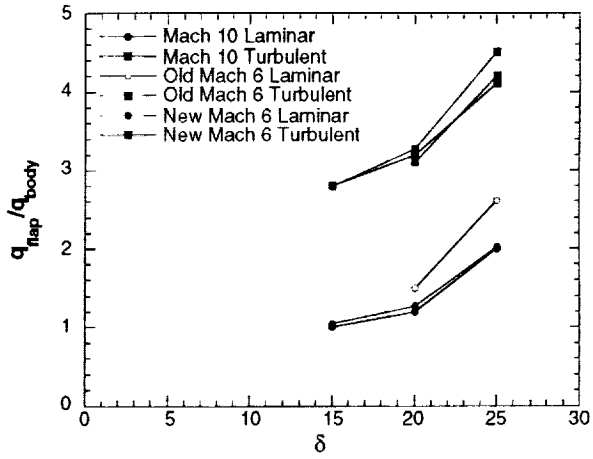

Figure 16. Body flap heating referenced to laminar forebody heating ahead of separation for α=40-deg.

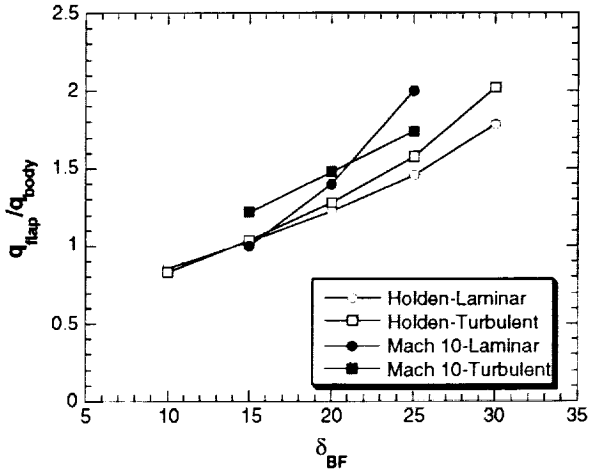

Figure 17. Comparison of Mach 10 body flap heating referenced to forebody heating ahead of separation against X-38 ATDB using Holden's method.

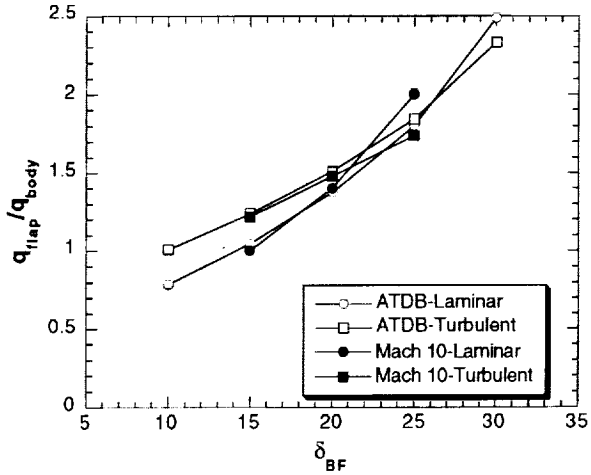

Figure 18. Comparison of Mach 10 body flap heating referenced to forebody heating ahead of separation against X-38 ATDB using current method.